Turbulence dissipation and the role of coherent structures in the near wake of a square prism

F. Alves Portela,* G. Papadakis, and J. C. Vassilicos†
Turbulence, Mixing and Flow Control Group, Department of Aeronautics, Imperial College London, London SW7 2AZ, United Kingdom

(Received 6 June 2018; published 26 December 2018)

Between streamwise distances $4d$ and at least $10d$ in the planar turbulent wake of a square prism of side length d, the turbulent fluctuating velocities are highly non-Gaussian, the turbulent energy spectrum has a close to $-5/3$ power law range, and the turbulence dissipation rate obeys the nonequilibrium dissipation scaling if the energy of the coherent structures is not included in the scaling. In this same range of streamwise distances, the coherent structure dissipation rate decays proportionally to the stochastic turbulence dissipation rate and there is a strong tendency of alignment or antialignment between fluctuating velocities and fluctuating vorticities which appears to coincide with the presence of coherent structures.

DOI: 10.1103/PhysRevFluids.3.124609

I. INTRODUCTION

The past decade has seen the emergence of a new turbulence dissipation scaling which is common to many turbulent flows (see [1,2]). This scaling is

$$C_\varepsilon \propto \frac{\sqrt{\mathrm{Re}_I}}{\mathrm{Re}_\lambda}, \tag{1}$$

where

$$C_\varepsilon \equiv \varepsilon \frac{\mathcal{L}}{\mathcal{U}^3}. \tag{2}$$

In Eq. (1), Re_I is an inlet or global Reynolds number and Re_λ is the Taylor length-based local Reynolds number. In Eq. (2), ε is the mean turbulent dissipation rate while $\mathcal{L}$ and $\mathcal{U}$ are, respectively, length and velocity scales associated with the largest turbulent eddies.

The scaling (1) has been found in important regions of various turbulent flows which extend over a number of turnover times and where well-defined $-5/3$ energy spectra exist: grid-generated turbulence (both fractal or multiscale and regular grids) [3–7], turbulent boundary layers [8], axisymmetric wakes [9–11], round and planar jets [12,13], and periodic turbulence, both forced and decaying [14]. In some of these flows, specifically grid-generated turbulence and decaying periodic turbulence, C_ε has been seen to become constant quite abruptly far enough downstream, but the direct numerical simulation (DNS) of [15] has shown that this constant C_ε is not a reflection of Kolmogorov equilibrium (in relation to which a constant C_ε is typically established) but of a balanced nonequilibrium.

*f.alves-portela@soton.ac.uk
†j.c.vassilicos@imperial.ac.uk

The purpose of the present paper is not to study what happens very far downstream where one might expect a transition to a Kolmogorov equilibrium constant C_ε in some cases (for example, in the case of planar jets where the local Reynolds number grows rather than decays with downstream distance) but to study how upstream the region where Eq. (1) holds can be. The present study differs substantially from the studies listed above because the focus is on a flow region where the fluctuating velocities are highly non-Gaussian and because some special attention is given to coherent structures. In fact, as will be seen below, the intense presence of coherent structures warrants careful definition of the velocity scale used to define C_ε.

A number of studies over the past five years have reported very-well-defined $-5/3$ energy spectra in the very near fields of grid-generated turbulence [6,16–21] and planar turbulent wakes [22]. In all these cases the $-5/3$ energy spectra are present in near-field regions where the turbulent fluctuating velocities are non-Gaussian and characterized by intense large-scale intermittency between potential and vortical flow. Given that the nonequilibrium turbulence dissipation scaling (1) exists in flow regions with well-defined $-5/3$ energy spectra, could it be that this scaling already exists at distances which are so close to the generating source of the turbulence (e.g., grid, bluff body, and jet nozzle) that turbulent fluctuating velocities are non-Gaussian? This is the primary question of this paper. It is addressed by analyzing DNS data of a turbulent planar wake generated by a square prism [22]. Our analysis focuses on the centerline near-field region between the square prism and a streamwise distance $10d$ from the prism, where d is the length of each side of the prism.

The second objective of this paper concerns the dissipative role of coherent structures. Goto and Vassilicos [15] argued that the nonequilibrium dissipation scaling (1) may be the result of some sort of locking between the dissipation rate of the large-scale coherent structures and the dissipation rate of the random turbulence fluctuations. Specifically, they proposed that Eq. (1) holds in flow regions where the influence of large-scale coherent structures is felt and where the dissipation associated with those structures ($\tilde{\varepsilon}$) evolves as a constant fraction of the stochastic turbulence dissipation (ε'), i.e., $\tilde{\varepsilon}/\varepsilon' = \text{const}$. Our second objective is to check whether this sort of balance is present in the region where we may detect Eq. (1) and perhaps also find some other complementary or related effects of coherent structures on the turbulence in this region.

In this paper we study data obtained by Alves Portela *et al.* [22] in their DNS of the turbulent planar wake of a square prism with inlet free-stream velocity U_∞ such that $\mathrm{Re}_I \equiv U_\infty d/\nu = 3900$ (ν is the fluid's kinematic viscosity). We refer to [22] for details of this DNS. Our study focuses on the turbulence dissipation and distinguishes between the coherent and stochastic parts of the fluctuating flow. In Sec. II we briefly explain how this distinction is made and document the non-Gaussianity of the flow. In Sec. III we address our primary objective and study the turbulence dissipation in terms of C_ε and of the triple decomposition introduced in Sec. II and in Sec. IV we address our secondary objective and explore the influence of the coherent motions on the turbulence dissipation. We summarize in Sec. V.

II. TRIPLE DECOMPOSITION AND NON-GAUSSIANITY OF THE FLOW

Coherent structures created by bluff bodies are easily identifiable through their periodic (or quasiperiodic) temporal signature, similar to the von Kármán street for laminar flows [23,24]. The task of extracting these structures is therefore rather simple, in contrast to other types of coherent structures with no such temporal signature. As proposed by Reynolds and Hussain [25,26], under such circumstances one can decompose the velocity and pressure signals into their mean ($\mathbf{U}$ and P), phase ($\tilde{\mathbf{u}}$ and $\tilde{p}$), and stochastic ($\mathbf{u}'$ and p') components. The turbulent fluctuating velocity is $\mathbf{u} = \tilde{\mathbf{u}} + \mathbf{u}'$. The operation $\langle\,\rangle$ is used to indicate time averaging (e.g., $\langle\mathbf{u}\rangle = 0$) and $\{\,\}$ is used to indicate phase averaging (e.g., $\{\mathbf{u}\} = \tilde{\mathbf{u}}$). The properties of the time- and phase-averaged signals can be found in Ref. [25].

The phase averaging is carried out by conditionally sampling the data based on a reference phase [27]. In the present work, a Hilbert transform is applied to the time signal of the lift coefficient. This yields a reference phase $\phi(t)$ associated with the vortex shedding because oscillations in

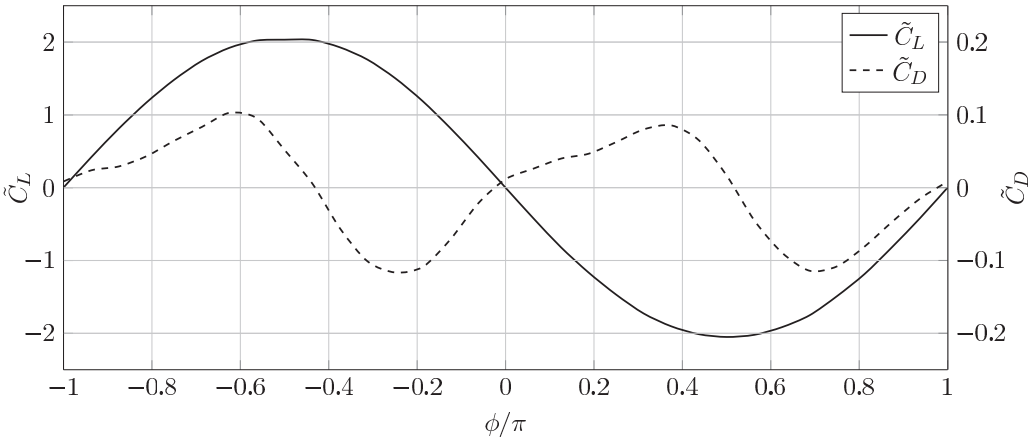

FIG. 1. Evolution of $\tilde{C}_L$ and $\tilde{C}_D$ along the phase ϕ normalized by π.

the force coefficients are related to the formation and departure of large-scale structures from the vortex formation region. In order to obtain phase-averaged quantities from our (discrete) data, it is necessary to bin $\phi(t)$ and then carry out a conditional averaging; the phase angle is discretized into 32 segments such that each time instant is associated with a phase $\phi = -\pi + n\frac{2\pi}{32}$, where $0 < n < 31$. Both the time- and the phase-averaging procedures involve averaging in the spanwise direction (normal to the plane of the average wake flow) in order to improve statistical convergence.

The resulting phase-averaged lift and drag coefficients $\tilde{C}_L$ and $\tilde{C}_D$, respectively, are shown in Fig. 1. Notice that $\tilde{C}_L$ follows a sine curve respecting the symmetry $\tilde{C}_L(\phi) = -\tilde{C}_L(\phi + \pi)$ and that $\tilde{C}_D$, albeit also periodic, displays the symmetry $\tilde{C}_D(\phi) = \tilde{C}_D(\phi + \pi)$ without following a cosine or sine wave.

Isovorticity contours and streamlines of the phase-averaged fluctuating velocity field $\tilde{\mathbf{u}}$ in the plane of the mean flow are shown in Fig. 2. The phase-averaged flow field displays a structure similar to that of the von Kármán vortex street (as highlighted in Ref. [23]) where the alternating vortices display opposite circulation. In Fig. 2 lines of constant vorticity are overlaid onto streamlines and indicate the presence of vortical coherent structures [28,29] in the fluctuating velocity field $\mathbf{u}$. This

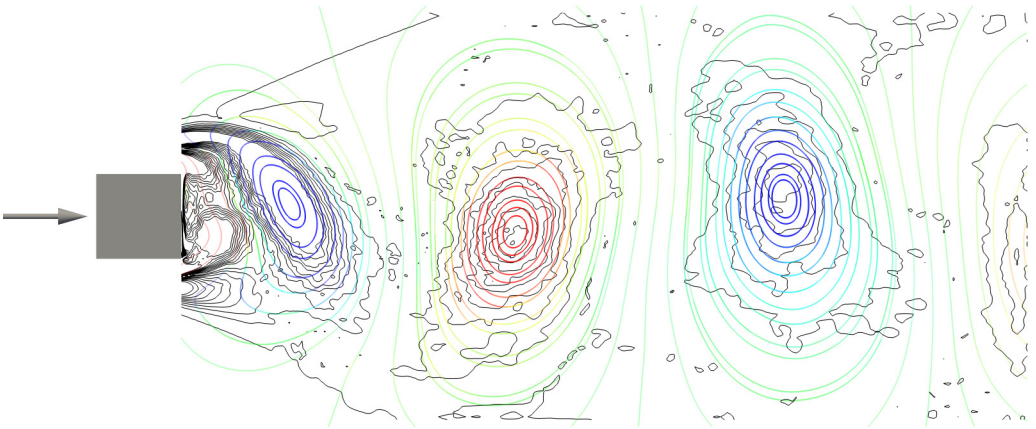

FIG. 2. Isovorticity (black lines) and streamlines of the phase-averaged fluctuating velocity field (color coded, blue for negative spanwise vorticity and red for positive spanwise vorticity) in the streamwise-transverse plane of the flow for an arbitrary phase. The arrow indicates the direction of the free-stream velocity.

coherent structures make the phase-averaged fluctuating velocity field $\tilde{\mathbf{u}}$. The difference between the two velocity fields is the stochastic velocity field $\mathbf{u}'$.

Taking x_1 to be the coordinate along the streamwise direction, i.e., the direction of the arrow in Fig. 2, the data available to us from the DNS of Alves Portela *et al.* [22] extend up to $x_1/d = 10$, the origin $x_1 = 0$ being at the center of the square prism. The centerline is in the streamwise direction and crosses the square prism exactly through the middle. In Fig. 3 one can see the probability density functions (PDFs) of fluctuating velocity components u_1 (in the streamwise direction), u_2 (in the cross-stream direction), and u_3 (in the spanwise direction normal to the plane of Fig. 2) and the PDFs of the stochastic fluctuating velocity components $u_1' \equiv u_1 - \{u_1\}$ and $u_2' \equiv u_2 - \{u_2\}$ ($u_3' = u_3$ because $\{u_3\} = 0$) at five different positions along the centerline. Clearly, u_1 and u_1' are near-Gaussian at $x_1/d \geqslant 4$ but not at $x_1/d = 2$ and u_2, u_2', and u_3 are very non-Gaussian for all $x_1 \leqslant 10$ on the centerline. The non-Gaussianity of u_2 may be traced back to the coherent structures as the double peaked PDF of u_2 arises from the strong cross-stream perturbations in the velocity of the fluid in between vortices. Notice, however, that u_3 is far from Gaussian even though it has no component associated with the coherent structures.

Alves Portela *et al.* [22] reported a well-defined $-5/3$ dependence on frequency of energy spectra at $x_1/d = 2$ over nearly one decade in this flow. They also reported power law dependences on frequency of energy spectra at $x_1/d > 2$ (their analysis did not extend beyond $x_1/d = 10$) but with power law exponent slightly steeper than $-5/3$, yet very close to $-5/3$ (see their Figs. 9 and 10). In the following section we study the dependence of C_ϵ on Re_λ in the near-field region $x_1/d \leqslant 10$ where the turbulence is demonstrably non-Gaussian and has energy spectra with close to $-5/3$ frequency scalings at $x_1/d \geqslant 2$. The turbulence dissipation scaling (1) has been reported in axisymmetric wakes in the range $10 \leqslant x_1/d \leqslant O(100)$ [10,11] and planar jets in the range $20 \leqslant x_1/d \leqslant O(100)$ [13], where d is the size of the wake generator in the case of the wake and the size of the nozzle exit in the case of the jet. The turbulence dissipation scaling is being investigated in the very near field $x_1/d \leqslant 10$ where the turbulence fluctuations are clearly documented to be very non-Gaussian.

III. COHERENT MOTIONS AND NONEQUILIBRIUM DISSIPATION

A. Energy and dissipation decompositions

One of the properties of the decomposition discussed above (see [25] for further details) is that the mean turbulent kinetic energy $k = \frac{1}{2}\langle u_i u_i \rangle$ is given by the sum of the coherent and stochastic components $\tilde{k} = \frac{1}{2}\langle \tilde{u}_i \tilde{u}_i \rangle$ and $k' = \frac{1}{2}\langle u_i' u_i' \rangle$, respectively. Likewise, the mean turbulent dissipation $\varepsilon = \nu \langle \frac{\partial u_i}{\partial x_j} \frac{\partial u_i}{\partial x_j} \rangle$ is given by the sum of the coherent and stochastic components $\tilde{\varepsilon} = \nu \langle \frac{\partial \tilde{u}_i}{\partial x_j} \frac{\partial \tilde{u}_i}{\partial x_j} \rangle$ and $\varepsilon' = \nu \langle \frac{\partial u_i'}{\partial x_j} \frac{\partial u_i'}{\partial x_j} \rangle$, respectively. These are shown in Fig. 4 along the geometrical centerline of the wake.

From Fig. 4 it is clear that the coherent motions contribute the largest portion of k. However, both $\tilde{k}$ and k' are of comparable magnitude throughout the region investigated here, even though $\tilde{k}$ has a steeper decay in the direction of the mean flow in comparison to k'. Hussain *et al.* [28,30] have made similar observations, albeit at much larger distances from the wake generator. Notice that while the energy contents of the coherent and stochastic motions are of comparable magnitudes, the dissipations associated with each of those motions, $\tilde{\varepsilon}$ and ε', respectively, are drastically different, and in fact $\tilde{\varepsilon} \ll \varepsilon'$ in agreement with [28,30].

B. Turbulence dissipation scaling

The definition of C_ε given in Eq. (2) involves a large-scale characteristic velocity $\mathcal{U}$ and a large-scale characteristic length $\mathcal{L}$ (see Table I). We define a Taylor length scale λ in terms of $\mathcal{U}$ as

$$\lambda = \sqrt{15\nu \frac{\mathcal{U}^2}{\varepsilon}} \tag{3}$$

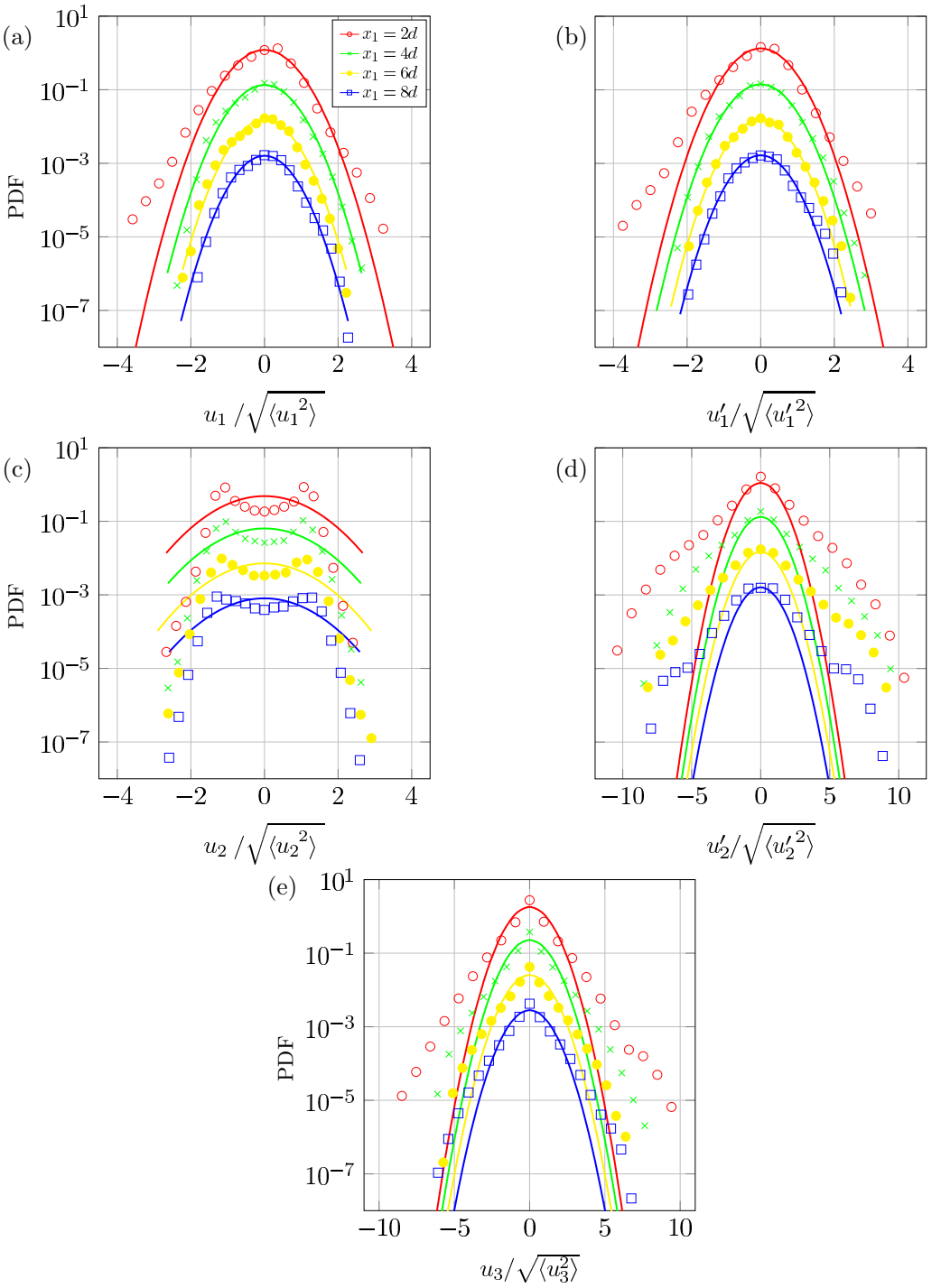

FIG. 3. PDFs of (a), (c), and (d) $u_i = \tilde{u}_i + u_i'$ (with $i = 1, 2, 3$, respectively) and (b) and (e) u_i' (with $i = 1, 2$, respectively) at $x_1/d = 2, 4, 6, 8$ on the geometric centerline. The PDFs are offset by a decade between consecutive locations. The solid lines show a Gaussian fit to the data.

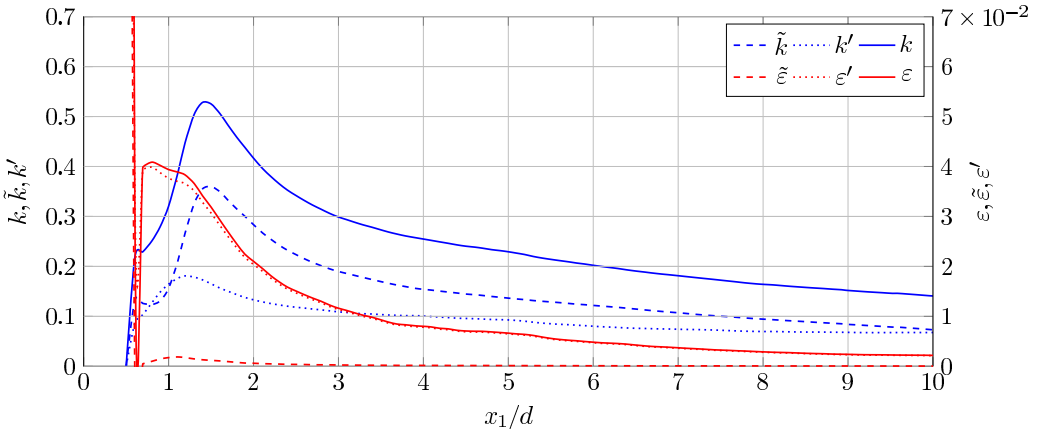

FIG. 4. Stochastic and coherent contributions to the turbulent kinetic energy (normalized by U_∞^2) and turbulent dissipation (normalized by U_∞^3/d).

and the corresponding Taylor length-based Reynolds number is

$$\mathrm{Re}_\lambda = \frac{\mathcal{U}\lambda}{\nu}. \tag{4}$$

This definition of λ is identical to the formula given by Taylor [31] for isotropic turbulence if $\mathcal{U} \equiv \sqrt{\langle u_1^2 \rangle}$. We return to our choice of definition of λ at the end of this section.

TABLE I. Mean values of quantities found to be approximately constant in the range $4 < x_1/d < 10$ (with the exception of the first three entries for which the mean values are calculated in the range $4 < x_1/d < 8$). The reported standard deviations and average departure from the mean relate to the spatial evolution (along x_1) of the respective time averaged quantities. The λ, given by Eq. (3), was computed with $\mathcal{U} = \sqrt{\langle u_1^2 \rangle}$.

Quantity	Mean value	Standard deviation	Average departure from mean
$U_1\Theta_{u_1'}/\mathcal{L}_{11}$	0.17	0.01	5.8%
$U_1\Theta_{u_1'}/\mathcal{L}_{21}$	0.32	0.02	5.1%
$U_1\Theta_{u_1'}/\mathcal{L}_{31}$	0.77	0.06	6.4%
C_ε with $\mathcal{U} = \sqrt{k}$	0.016	0.001	4.7%
Re_λ with $\mathcal{U} = \sqrt{k}$	717.7	24	2.9%
$C_\varepsilon \mathrm{Re}_\lambda$ with $\mathcal{U} = \sqrt{k}$	11.2	0.5	3.6%
λ_{11}/λ	1.4	0.03	1.9%
λ_{12}/λ	0.97	0.02	1.4%
λ_{13}/λ	0.98	0.04	3.5%
λ_{21}/λ	2.1	0.06	2.4%
λ_{22}/λ	2.8	0.12	3.3%
λ_{23}/λ	2	0.13	5.7%
λ_{31}/λ	0.62	0.02	2.1%
λ_{32}/λ	0.57	0.02	3.3%
λ_{33}/λ	0.78	0.02	2.9%
$\mathcal{L}/\lambda_{11}$	0.86	0.07	5.9%
$\mathcal{L}/\lambda_{22}$	0.44	0.02	3.9%
$\mathcal{L}/\lambda_{23}$	0.61	0.03	4.1%
$\mathcal{L}/\lambda$	1.23	0.07	4.4%

From Eqs. (2) and (3) it immediately follows that $\mathcal{L}/\lambda \sim C_\epsilon \mathrm{Re}_\lambda$. Given that all the quantities in this relation are local in space, it implies, in particular, that $\mathcal{L}/\lambda$ and $C_\epsilon \mathrm{Re}_\lambda$ vary in the same way along the centerline of the flow. To check what these variations are we need to define $\mathcal{L}$ and $\mathcal{U}$.

Following Taylor [31], $\mathcal{L}$ should be an integral length scale such as

$$\mathcal{L}_{ij} = \frac{1}{\langle u_i'(\mathbf{x}, t)^2 \rangle} \int_{-\infty}^{\infty} \langle u_i'(\mathbf{x}, t) u_i'(\mathbf{x} + \xi \mathbf{e}_j, t) \rangle d\xi, \tag{5}$$

where there is no summation over repeated indices and $\mathbf{e}_j$ is a unit vector in the direction measured by x_j. Practical usage of Eq. (5) is impaired by the fact that the autocorrelations of the different velocity components reach zero only at very large ξ especially when $\mathbf{e}_j$ is aligned with the cross-stream and spanwise directions, as is indeed the case in our simulations. If $\mathbf{e}_j$ is aligned with the free-stream direction, i.e., $j = 1$, the extent of the domain over which $\mathcal{L}_{i1}$ can be computed is limited between $x_1/d = 3$ and $x_1/d = 8$. In this part of the computational domain it was possible to compute these length scales by taking the limits of the integral in Eq. (5) to be the first zero crossings of the integrand. We calculated $U_1 \Theta_{u_1'}$ divided by $\mathcal{L}_{i1}$ for $i = 1, 2, 3$ on the part of the centerline where the integral scales $\mathcal{L}_{i1}$ were computable; $U_1 \Theta_{u_1'}$ is the product of the mean streamwise velocity and the integral time scale associated with u_1', i.e.,

$$\Theta_{u_1'}(\mathbf{x}) = \frac{1}{\langle u_1'(\mathbf{x}, t)^2 \rangle} \int_{0}^{\infty} \langle u_1'(\mathbf{x}, t) u_1'(\mathbf{x}, t + \tau) \rangle d\tau. \tag{6}$$

The ratios $U_1 \Theta_{u_1'}/\mathcal{L}_{i1}$ were found to be roughly constant for any i in the range $4 < x_1/d < 8$; they do not follow any clear trend with x_1/d and depart, on average, from their constant mean values by no more than 6.4% (see Table I). Hence, making the choice $\mathcal{L} = U_1 \Theta_{u_1'}$ affects the computation of C_ε only in terms of its values but not in terms of its dependence on x_1/d because the evolution of $U_1 \Theta_{u_1'}$ with x_1/d closely coincides with that of $\mathcal{L}_{i1}$ (for all i). Furthermore, $U_1 \Theta_{u_1'}$ can be calculated throughout our domain whereas $\mathcal{L}_{i1}$ cannot. In the remainder of this paper we therefore set $\mathcal{L} = U_1 \Theta_{u_1'}$.

The first natural candidate for our choice of $\mathcal{U}$ is $\mathcal{U} = k^{1/2}$. This choice was found to lead to C_ε and Re_λ both being approximately constant on the centerline region $x_1/d \gtrsim 4$, i.e., just downstream of the vortex formation region. The product $C_\varepsilon \mathrm{Re}_\lambda$ is therefore also constant in this region, as reported in Table I, and it is impossible to distinguish between $C_\varepsilon = \text{const}$ and $C_\varepsilon \sim \mathrm{Re}_\lambda^{-1}$. The constancy of C_ε, Re_λ, and $C_\varepsilon \mathrm{Re}_\lambda$ in the range $4 < x_1/d < 10$ was found to be within 3%–5% of their respective mean values over this range. This of course neither confirms nor invalidates anything since one needs Re_λ to vary along x_1/d in order to conclude on the behavior of C_ε.

Recall from Fig. 4 that $\tilde{k}$ decays at a faster rate than k' along the centerline of the wake. This suggests that $\mathrm{Re}_\lambda \approx \text{const}$ may be a result of our choice of $\mathcal{U}$. Indeed, the difference between the decays of $\tilde{k}$ and k' with x_1/d was found to be mostly caused by $\langle \tilde{u}_2^2 \rangle$, which is much larger and decays faster than $\langle u_2'^2 \rangle$. Thus, the observation that both C_ε and Re_λ are approximately constant may be a result of choosing a velocity scale which is heavily affected by the vortex shedding.

The natural candidate for our choice of $\mathcal{U}$ if we want to disregard vortex shedding effects is $\mathcal{U} = k'^{1/2}$. In fact, any large-scale velocity scale $\mathcal{U}$ which does not include $\sqrt{\langle \tilde{u}_2^2 \rangle}$ is equally well suited to the task given that $\langle u_1^2 \rangle / k'^{1/2}$, $\langle u_3^2 \rangle / k'^{1/2}$, and $\langle u_i'^2 \rangle / k'^{1/2}$, for all i, are approximately constant for $x_1/d \gtrsim 4$ (see Fig. 5). Each one of these ratios varies by less than 2% of their respective mean in that range.

The values of C_ε and Re_λ resulting from $\mathcal{U} = k'^{1/2}$ are plotted in Fig. 6 as functions of streamwise distance from the prism along the centerline. The local Reynolds number Re_λ and the dissipation coefficient C_ε now vary significantly with x_1/d, the former increasing and the latter decreasing with growing x_1/d from about $x_1/d \gtrsim 2$. In fact, as shown in Fig. 7, the product $C_\varepsilon \mathrm{Re}_\lambda$ is approximately constant in the range $4 \lesssim x_1/d \lesssim 10$, i.e., from just downstream of the vortex formation region to the

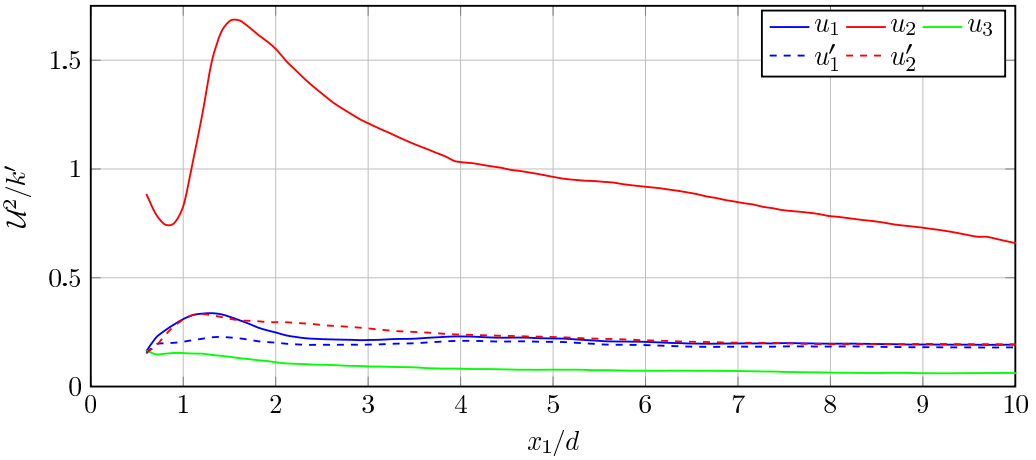

FIG. 5. Ratio between different definitions of the velocity scale $\mathcal{U}$ and the mean turbulent kinetic energy associated with the stochastic motions.

end of our database. The average deviation of $C_\varepsilon \mathrm{Re}_\lambda$ from its mean value in the range $4 \leqslant x_1/d \leqslant 10$ is about 4% (in fact, the difference between $C_\varepsilon \mathrm{Re}_\lambda$ at $x_1/d = 4$ and $x_1/d = 10$ is about 1% of the mean value in that range), whereas in Fig. 6 the deviations of C_ε and Re_λ from their mean values in the same range are about 9% and 13%, respectively, with C_ε decreasing with x_1 whereas Re_λ increases. We can therefore safely conclude that $C_\varepsilon \sim \mathrm{Re}_\lambda^{-1}$ holds in the near field $4 \lesssim x_1/d \lesssim 10$ if $\mathcal{U}$ is defined in a way which does not significantly involve the large-scale coherent structures.

Even though the streamwise extent of our database may appear to be relatively small, it does cover a significant number of eddy turnover times

$$\mathcal{E} = \int_{x_a}^{x_b} U_1^{-1} \frac{\mathcal{U}}{\mathcal{L}} dx, \tag{7}$$

where x_a and x_b are two different streamwise locations along the centerline of the flow and $\mathcal{U} = k'^{1/2}$. For $x_a/d = 2$ and $x_b/d = 4$ one has $\mathcal{E} \approx 2.7$, while for $x_a/d = 4$ and $x_b/d = 10$ (the furthest location available in our database) one has $\mathcal{E} \approx 7.3$. This inspires confidence in the relevance of

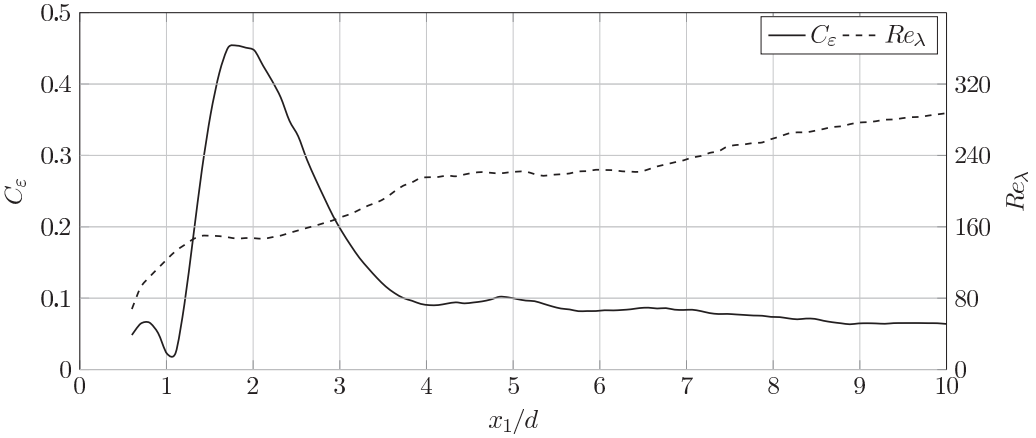

FIG. 6. Evolution of C_ε and Re_λ along the centerline using $\mathcal{U} = k'^{1/2}$.

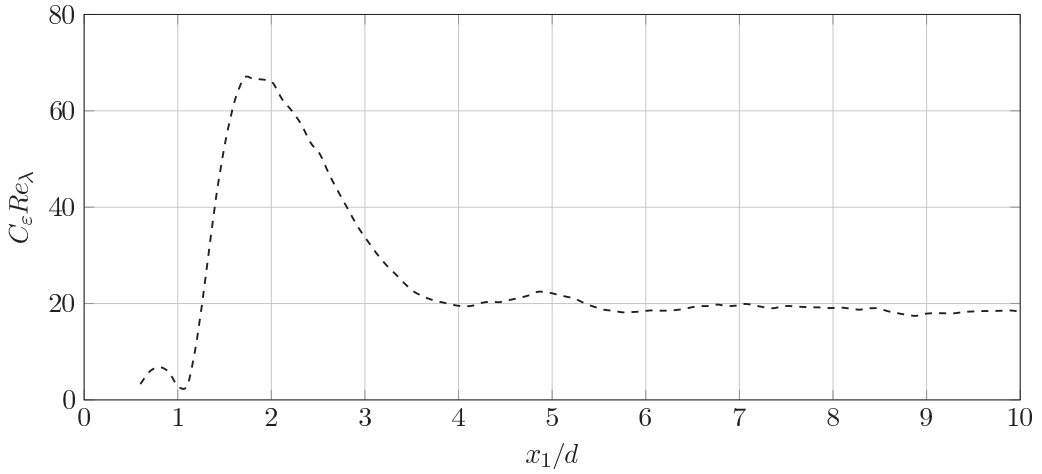

FIG. 7. Evolution of $C_\varepsilon \mathrm{Re}_\lambda$ along the centerline using $\mathcal{U} = k'^{1/2}$.

$C_\varepsilon \propto \mathrm{Re}_\lambda^{-1}$, which is seen in our simulation (Fig. 7) in a region of space which may appear small but nevertheless represents a considerable number of eddy turnover times.

At the beginning of this section the Taylor length λ was defined by Eq. (3). This definition was used to calculate C_ε and Re_λ with $\mathcal{U} = k^{1/2}$ in Table I and with $\mathcal{U} = k'^{1/2}$ in Figs. 6 and 7. One can ask how our conclusion that $C_\varepsilon \sim \mathrm{Re}_\lambda^{-1}$ might change if we were to choose a different definition for the Taylor length, for example, any of the following λ_{ij} defined as

$$\lambda_{ij} = \sqrt{\frac{2\langle u_i^2 \rangle}{\left\langle \left(\frac{\partial u_i}{\partial x_j}\right)^2 \right\rangle}} \tag{8}$$

without summing over repeated indices.

The different estimates λ_{ij} of the Taylor length were computed and compared to the isotropic estimate λ given by Eq. (3). The ratios λ_{ij}/λ were found to be approximately constant in the range $4 \lesssim x_1/d < 10$, as reported in Table I. Even though the different scales given by Eq. (8) do not satisfy isotropy (i.e., $\lambda_{11} \neq \lambda_{22} \neq \lambda_{33}$ and $\lambda_{12} \approx \lambda_{13} \neq \lambda_{21} \approx \lambda_{23} \neq \lambda_{31} \approx \lambda_{32}$ and also $\lambda_{11} \neq 2\lambda_{12}$ and $\lambda_{11} \neq 2\lambda_{13}$), all combinations of i and j used in Eq. (8) consistently appear to be approximately proportional to λ in the range $4 \lesssim x_1/d < 10$. We in fact confirmed that use of λ_{ij} instead of λ in the calculation of Re_λ leads to plots qualitatively similar to Figs. 6 and 7 and that $C_\varepsilon \mathrm{Re}_\lambda$ remains constant in the range $4 \lesssim x_1/d < 10$ within the same degree of confidence as when λ is used. This is confirmed by the constancy of the ratios $\mathcal{L}/\lambda_{ij}$ which, as shown in Table I, are only different in magnitude, remaining practically constant with growing x_1/d for $x_1/d \gtrsim 4$.

This section's conclusion is that, for the inlet Reynolds number $\mathrm{Re}_I = 3900$ considered here, Eq. (1) holds in the near-field range $x_1/d \approx 4$ to $x_1/d = 10$ where the turbulence is highly non-Gaussian provided that the velocity scale $\mathcal{U}$ characterizing the turbulence fluctuations does not include any significant contribution from the large-scale coherent structures. Other than this, there seems to be no restriction on the choice of $\mathcal{L}$ and the Taylor length scale. The different choices of these length scales that we were able to test only changed the constant of proportionality in Eq. (1) but not significantly the functional dependence.

IV. LINK BETWEEN COHERENT AND STOCHASTIC MOTIONS

Goto and Vassilicos [15] argued that the nonequilibrium dissipation scaling $C_\varepsilon \sim \mathrm{Re}_\lambda^{-1}$ may result from a locking between the dissipation rates of the coherent and the stochastic turbulent motions. Even though $\tilde{\varepsilon}$ is much smaller than ε', in the present case about 40 times smaller, Goto and

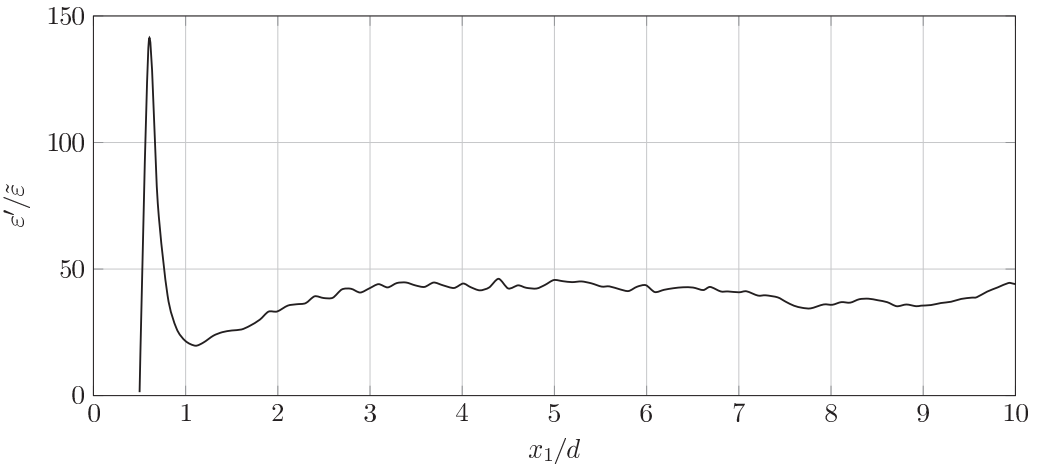

FIG. 8. Ratio between the dissipation ε' associated with the stochastic component and the dissipation $\tilde{\varepsilon}$ associated with the phase component as a function of x_1/d on the centerline.

Vassilicos [15] hypothesized that the ratio between these two quantities may remain about constant during some of the evolution of the turbulence, i.e., along some of the streamwise direction in the present case, and argued that this constancy is the cause behind the scaling $C_\varepsilon \sim \mathrm{Re}_\lambda^{-1}$. In Fig. 8 we plot $\varepsilon'/\tilde{\varepsilon}$ along the centerline and find that this ratio is indeed approximately constant from $x_1/d \approx 4$ to $x_1/d = 10$, i.e., nearly exactly where we also demonstrate the validity of $C_\varepsilon \sim \mathrm{Re}_\lambda^{-1}$ for the present data. While we cannot establish a causal relation between the constancy of $\varepsilon'/\tilde{\varepsilon}$ and $C_\varepsilon \sim \mathrm{Re}_\lambda^{-1}$ at this stage, it does certainly appear that both hold over the same range of streamwise distances in our flow. A related observation has already been made in a DNS of decaying turbulence in a periodic box by Goto and Vassilicos [15].

The dissipation of the stochastic turbulent fluctuations results from a nonlinear cascade of turbulent kinetic energy. If it is somehow locked to the dissipation of the coherent fluctuations then one should be able to see an effect of these fluctuations on the stochastic motions. Such an effect and the proportionality between ε' and $\tilde{\varepsilon}$ require a full study of their own, which is beyond this paper's scope. However, we close this work by providing in the following two figures a few suggestive results along these lines which we hope will stimulate further study.

The nonlinearity in the Navier-Stokes equations is essentially the Lamb vector $\boldsymbol{\omega} \times \mathbf{u}$ (where $\boldsymbol{\omega} \equiv \boldsymbol{\nabla} \times \mathbf{u}$) because $\mathbf{u} \cdot \boldsymbol{\nabla}\mathbf{u}$ can be decomposed into this vector and the gradient of $|\mathbf{u}|^2/2$. The Reynolds stress term appears in the Reynolds-averaged Navier-Stokes (RANS) equation as the average of the Lamb vector plus the gradient of the average of $|\mathbf{u}|^2/2$, which can therefore be subsumed into the pressure. The Lamb vector is therefore responsible for the turbulence effects on the mean flow and for the nonlinear cascade which causes these fluctuations to dissipate.

It is simpler to look at the helicity $h = \mathbf{u} \cdot \boldsymbol{\omega}$ and in particular the relative helicity

$$\hat{h} = \frac{h}{\|\mathbf{u}\| \cdot \|\boldsymbol{\omega}\|} = \cos[\angle(\mathbf{u}, \boldsymbol{\omega})], \tag{9}$$

which are both scalars, rather than the Lamb vector. This is what we do to end this paper because values close to ± 1 of the relative helicity translate into zero Lamb vectors, i.e., to depletion of nonlinearity, turbulence cascade, and turbulence dissipation and also depletion of the turbulence damping term in the RANS equation. The relative helicity contains the part of h which depends solely on the alignment between the fluctuating velocity $\mathbf{u}$ and the fluctuating vorticity $\boldsymbol{\omega}$. Under the decomposition introduced in Sec. II, one can see that h is the sum of four contributions

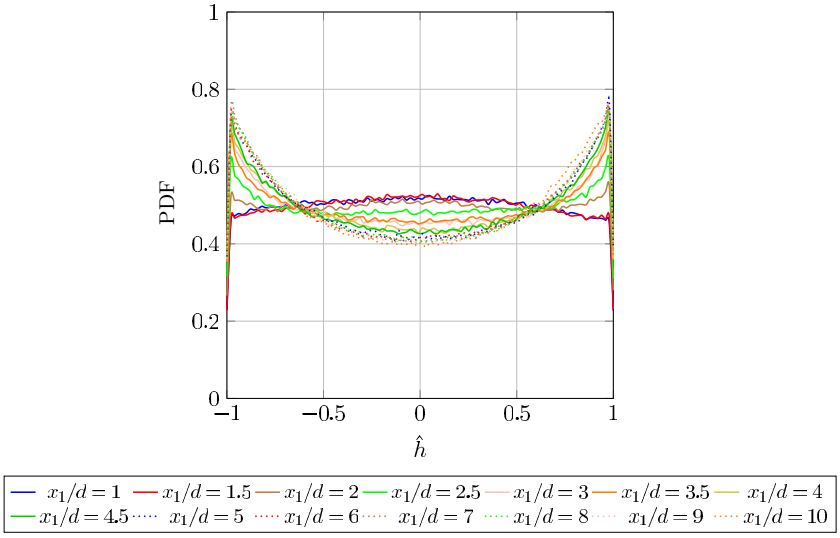

FIG. 9. PDFs of the relative helicity $\hat{h}$ at different locations on the centerline.

$h = h_{ss} + h_{cc} + h_{cs} + h_{sc}$, where

$$h_{ss} = \mathbf{u}' \cdot \boldsymbol{\omega}', \tag{10a}$$

$$h_{cc} = \tilde{\mathbf{u}} \cdot \tilde{\boldsymbol{\omega}}, \tag{10b}$$

$$h_{cs} = \tilde{\mathbf{u}} \cdot \boldsymbol{\omega}', \tag{10c}$$

$$h_{sc} = \mathbf{u}' \cdot \tilde{\boldsymbol{\omega}}. \tag{10d}$$

Each one of these four quantities has an associated relative helicity defined in a similar way as Eq. (9). Zhou *et al.* [20] reported interesting results on the helicity and relative helicity along the centerline of a single square grid flow which is mostly potential in the very near field and therefore very different from the present near field and did not consider the decomposition $h = h_{ss} + h_{cc} + h_{cs} + h_{sc}$.

As in the preceding section, our focus is only on the geometric centerline of the wake. The mean values of Eqs. (10a)–(10d) were found to be uniformly zero at all the points on the centerline where we calculated these mean values. The standard deviation of h_{cc} is zero because $h_{cc} = 0$ by construction and the standard deviation of h_{sc} was found to be negligible compared to the standard deviations of h_{ss} and h_{cs}. Hence, $\langle h^2 \rangle \approx \langle h_{cs}^2 \rangle + \langle h_{ss}^2 \rangle$.

Figure 9 shows the PDF of $\hat{h}$ at different locations on the centerline. Very close to the prism, the PDF of $\hat{h}$ is approximately uniform. At $x_1/d \approx 2$ peaks start to develop at $\hat{h} = \pm 1$. Further away from the prism these peaks become more pronounced and the PDFs become clearly bimodal at $x_1/d \gtrsim 4$. Even though the dissipation decreases continuously with distance to the prism (recall Fig. 4) the ratio $\varepsilon'/\tilde{\varepsilon}$ acquires at $x_1/d \gtrsim 4$ the approximately constant value that it keeps until $x_1/d \gtrsim 10$. The tendency of alignment and antialignment between the vectors $\mathbf{u}$ and $\boldsymbol{\omega}$ coincides with the constancy of $\varepsilon'/\tilde{\varepsilon}$.

The results shown in Fig. 9 are similar to those of Rogers and Moin [32] when moving from the buffer layer towards the symmetry plane of a turbulent channel flow. Even though Rogers and Moin [32] argue that any link between coherent structures and h may be tenuous, Hussain *et al.* [30] link the coherent structures observed near the symmetry plane of turbulent channel flows to those observed in mixing layer. These structures are essentially spanwise rollers similar to those found in the present flow.

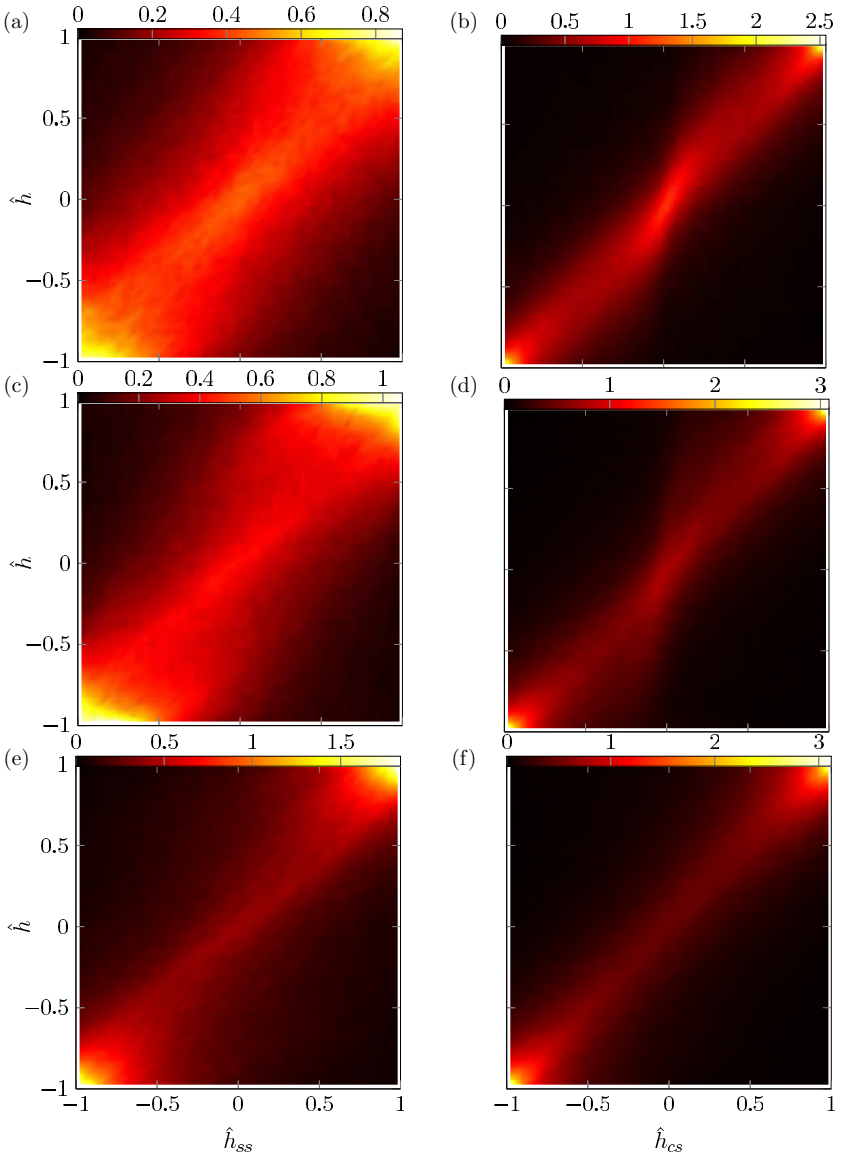

FIG. 10. Joint PDFs of $\hat{h}$ with both $\hat{h}_{ss}$ (left column) and $\hat{h}_{cs}$ (right column) for (a) and (b) $x_1/d = 2$, (c) and (d) $x_1/d = 4$, and (e) and (f) $x_1/d = 10$.

The main contributions to $\langle h^2 \rangle$ are $\langle h_{ss}^2 \rangle$ and $\langle h_{cs}^2 \rangle$ and it is natural to ask whether the alignment and antialignment between $\mathbf{u}$ and $\boldsymbol{\omega}$ originate from an alignment and antialignment between $\tilde{\mathbf{u}}$ and $\boldsymbol{\omega}'$ or/and from an alignment and antialignment between $\mathbf{u}'$ and $\boldsymbol{\omega}'$. We checked that no particular alignment and antialignment exists between $\mathbf{u}'$ and $\tilde{\boldsymbol{\omega}}$.

To answer this question we plot in Fig. 10 joint PDFs of $\hat{h}$ and $\hat{h}_{ss}$ on the left and joint PDFs of $\hat{h}$ and $\hat{h}_{cs}$ on the right at three centerline positions $x_1/d = 2, 4, 10$. These PDFs exhibit clear peaks at $(-1, -1)$ and (1,1) (in yellow) and appear concentrated along the bisector of the first and fourth quadrants, indicating a significant degree of correlation between $\hat{h}$ and $\hat{h}_{cs}$ on the one hand and between $\hat{h}$ and $\hat{h}_{ss}$ on the other. However, contrasting Figs. 10(a), 10(c), and 10(e) with

Figs. 10(b), 10(d), and 10(f) reveals that the latter are sharper. Furthermore, at the peaks [i.e., at the pairs $(-1, 1)$ and (1,1)] the values of the joint PDF of $\hat{h}$ and $\hat{h}_{cs}$ are at least twice as large as the values of the joint PDF of $\hat{h}$ and $\hat{h}_{ss}$. This suggests that the coherent structures do indeed have an effect on the stochastic turbulence fluctuations, in fact by organizing them around themselves in a way which increases the likelihood of maximum magnitudes of the relative helicities $\hat{h}_{cs}$, $\hat{h}$, and even, to some extent, $\hat{h}_{ss}$. We can therefore conclude that the coherent structures do seem to cause a depletion of nonlinearity which can be expected to interfere with the turbulence cascade and thereby with the turbulence dissipation, in a way which may be causing or contributing to the constancy of $\varepsilon'/\tilde{\varepsilon}$ observed in the streamwise centerline region where we also observe the dissipation scaling $C_\varepsilon \sim Re_\lambda^{-1}$. Note that the near $-5/3$ energy spectra at these very positions of this exact same flow [22] are present irrespective of this partial depletion of nonlinearity.

V. CONCLUSION

We studied a near-field turbulent flow which is not only inhomogeneous, given its proximity to the wake generator, but also anisotropic, including at the smallest scales. In fact, we have shown that the turbulence in the near field we studied here is also highly non-Gaussian, even the stochastic component of the turbulence on its own. However, Alves Portela *et al.* [22] reported well-defined close to $-5/3$ energy spectra in this near-field region. Here we found that the nonequilibrium dissipation scaling (1) holds in this near-field range ($x_1/d \approx 4$ to $x_1/d = 10$) if the velocity scale $\mathcal{U}$ characterizing the turbulence fluctuations does not include any significant contribution from the large-scale coherent structures. Previous works have revealed the presence of the nonequilibrium dissipation scaling (1) without the need to remove the coherent structure signature from the scaling quantities, in regions of evolving turbulent flows where the turbulence was either documented to have large-scale Gaussianity and small-scale isotropy or can reasonably be expected to have these two characteristics (see references given in the Introduction). This nonequilibrium dissipation scaling was even previously found in time-evolving periodic turbulence which can be considered to be analogous to homogeneous turbulence. The only significant commonality between the present near-field region and the regions where the nonequilibrium dissipation scaling (1) was found in previous studies is the presence of approximately $-5/3$ turbulent energy spectra.

Our near-field data support the hypothesis introduced by Goto and Vassilicos [15] that the dissipation rates of the coherent and the incoherent fluctuations decay together as if they were somehow locked to each other, i.e., that $\varepsilon'/\tilde{\varepsilon}$ remains about constant, in the region where the dissipation scaling $C_\varepsilon \sim \mathrm{Re}_\lambda^{-1}$ holds. This constant ratio suggests a link between the large-scale coherent motions and the stochastic turbulence cascade. We attempted to substantiate this notion by demonstrating a clear tendency for the fluctuating velocity field to align or antialign with the fluctuating vorticity field in this near-field region and that this tendency is highly correlated with another tendency which is also present, alignment or antialignment of coherent fluctuating velocity with stochastic fluctuating vorticity. However, this is only an indicative beginning and much work remains to be done to uncover the nature of the interactions between large-scale coherence and turbulence cascade. The indications are that these interactions may be responsible for the nonequilibrium dissipation scaling.

ACKNOWLEDGMENTS

The authors acknowledge the EU support through the FP7 Marie Curie MULTISOLVE project (Grant No. 317269), the computational resources allocated in ARCHER HPC through the UKTC funded by the EPSRC Grant No. EP/L000261/1, and the HPC resources provided by Imperial College on the cx2 facility. J.C.V. also acknowledges the support of an ERC Advanced Grant (Grant No. 320560).

[1] J. C. Vassilicos, Dissipation in turbulent flows, Annu. Rev. Fluid Mech. **47**, 95 (2015).
[2] I. P. Castro, Dissipative distinctions, J. Fluid Mech. **788**, 1 (2016).
[3] R. E. Seoud and J. C. Vassilicos, Dissipation and decay of fractal-generated turbulence, Phys. Fluids **19**, 105108 (2007).
[4] P. C. Valente and J. C. Vassilicos, The non-equilibrium region of grid-generated decaying turbulence, J. Fluid Mech. **744**, 5 (2014).
[5] N. Mazellier and J. C. Vassilicos, The turbulence dissipation constant is not universal because of its universal dependence on large-scale flow topology, Phys. Fluids **20**, 015101 (2008).
[6] R. J. Hearst and P. Lavoie, Decay of turbulence generated by a square-fractal-element grid, J. Fluid Mech. **741**, 567 (2014).
[7] K. Nagata, Y. Sakai, T. Inaba, H. Suzuki, and O. Terashima, Turbulence structure and turbulence kinetic energy transport in multiscale/fractal-generated turbulence, Phys. Fluids **25**, 065102 (2013).
[8] J. Nedić, S. Tavoularis, and I. Marusic, Dissipation scaling in constant-pressure turbulent boundary layers, Phys. Rev. Fluids **2**, 032601 (2017).
[9] J. Nedić, J. C. Vassilicos, and B. Ganapathisubramani, Axisymmetric Turbulent Wakes with New Nonequilibrium Similarity Scalings, Phys. Rev. Lett. **111**, 144503 (2013).
[10] T. Dairay, M. Obligado, and J. C. Vassilicos, Non-equilibrium scaling laws in axisymmetric turbulent wakes, J. Fluid Mech. **781**, 166 (2015).
[11] M. Obligado, T. Dairay, and J. C. Vassilicos, Nonequilibrium scalings of turbulent wakes, Phys. Rev. Fluids **1**, 044409 (2016).
[12] M. Breda and O. Buxton, Influence of coherent structures on the evolution of an axisymmetric turbulent jet, Phys. Fluids **30**, 035109 (2018).
[13] G. Cafiero and J. C. Vassilicos, Non-equilibrium turbulence scalings and self-similarity in turbulent planar jets, arXiv:1803.10488 [J. Fluid Mech. (unpublished)].
[14] S. Goto and J. C. Vassilicos, Energy dissipation and flux laws for unsteady turbulence, Phys. Lett. A **379**, 1144 (2015).
[15] S. Goto and J. C. Vassilicos, Unsteady turbulence cascades, Phys. Rev. E **94**, 053108 (2016).
[16] S. Laizet, J. C. Vassilicos, and C. Cambon, Interscale energy transfer in decaying turbulence and vorticity-strain-rate dynamics in grid-generated turbulence, Fluid Dyn. Res. **45**, 061408 (2013).
[17] J. C. Isaza, R. Salazar, and Z. Warhaft, On grid-generated turbulence in the near- and far field regions, J. Fluid Mech. **753**, 402 (2014).
[18] S. Laizet, J. Nedić, and J. C. Vassilicos, The spatial origin of $-5/3$ spectra in grid-generated turbulence, Phys. Fluids **27**, 065115 (2015).
[19] R. Gomes-Fernandes, B. Ganapathisubramani, and J. C. Vassilicos, The energy cascade in near-field non-homogeneous non-isotropic turbulence, J. Fluid Mech. **771**, 676 (2015).
[20] Y. Zhou, K. Nagata, Y. Sakai, Y. Ito, and T. Hayase, Spatial evolution of the helical behavior and the $2/3$ power-law in single-square-grid-generated turbulence, Fluid Dyn. Res. **48**, 021404 (2016).
[21] I. Paul, G. Papadakis, and J. C. Vassilicos, Genesis and evolution of velocity gradients in near-field spatially developing turbulence, J. Fluid Mech. **815**, 295 (2017).
[22] F. Alves Portela, G. Papadakis, and J. C. Vassilicos, The turbulence cascade in the near wake of a square prism, J. Fluid Mech. **825**, 315 (2017).
[23] T. von Kármán, *Aerodynamics* (McGraw-Hill, New York, 1963).
[24] A. Roshko, On the development of turbulent wakes from vortex streets, Ph.D. thesis, California Institute of Technology, 1952.
[25] W. C. Reynolds and A. K. M. F. Hussain, The mechanics of an organized wave in turbulent shear flow. Part 3. Theoretical models and comparisons with experiments, J. Fluid Mech. **54**, 263 (1972).
[26] A. K. M. F. Hussain and W. C. Reynolds, The mechanics of an organized wave in turbulent shear flow, J. Fluid Mech. **41**, 241 (1970).
[27] R. W. Wlezien and J. L. Way, Techniques for the experimental investigation of the near wake of a circular cylinder, AIAA J. **17**, 563 (1979).
[28] A. K. M. F. Hussain, Coherent structures-reality and myth, Phys. Fluids **26**, 2816 (1983).

[29] D. A. Lyn, S. Einav, W. Rodi, and J. H. Park, A laser-Doppler velocimetry study of ensemble-averaged characteristics of the turbulent near wake of a square cylinder, J. Fluid Mech. **304**, 285 (1995).
[30] A. K. M. F. Hussain, J. Jeong, and J. Kim, *Proceedings of the 1987 Summer Program on Studying Turbulence Using Numerical Simulation Databases* (Stanford University, Stanford, 1987).
[31] G. I. Taylor, Statistical theory of turbulence, Proc. R. Soc. London Ser. A **151**, 421 (1935).
[32] M. M. Rogers and P. Moin, Helicity fluctuations in incompressible turbulent flows, Phys. Fluids **30**, 2662 (1987).